Title
Advances in understanding the generation and evolution of the toroidal rotation profile on DIII-D

Journal
Nuclear Fusion, 49(8)

ISSN
0029-5515

Authors
Solomon, WM
Burrell, KH
Garofalo, AM
et al.

Publication Date
2009-08-01

DOI
10.1088/0029-5515/49/8/085005

IOP Publishing and International Atomic Energy Agency Nuclear Fusion

Nucl. Fusion **49** (2009) 085005 (11pp) doi:10.1088/0029-5515/49/8/085005

Advances in understanding the generation and evolution of the toroidal rotation profile on DIII-D

W.M. Solomon[1], K.H. Burrell[2], A.M. Garofalo[2], A.J. Cole[3], R.V. Budny[1], J.S. deGrassie[2], W.W. Heidbrink[4], G.L. Jackson[2], M.J. Lanctot[5], R. Nazikian[1], H. Reimerdes[5], E.J. Strait[2], M.A. Van Zeeland[2] and the DIII-D Rotation Physics Task Force

[1] Princeton Plasma Physics Laboratory, Princeton University, Princeton, NJ 08543, USA
[2] General Atomics, PO Box 85608, San Diego, CA 92186-5608, USA
[3] University of Wisconsin-Madison, Madison, WI 53706-1609, USA
[4] University of California-Irvine, Irvine, CA 92697, USA
[5] Columbia University, New York, NY 10027, USA

E-mail: wsolomon@pppl.gov

Received 14 January 2009, accepted for publication 22 May 2009
Published 7 July 2009
Online at stacks.iop.org/NF/49/085005

Abstract
Recent experiments using DIII-D's capability to vary the injected torque at constant power have focused on developing the physics basis for understanding rotation through the detailed study of momentum sources, sinks and transport. Non-resonant magnetic braking has generally been considered a sink of momentum; however, recent results from DIII-D suggest that it may also act as a source. The torque applied by the field depends on the rotation relative to a non-zero 'offset' rotation. Therefore, at low initial rotation, the application of non-resonant magnetic fields can actually result in a spin-up of the plasma. Direct evidence of the effect of reverse shear Alfvén eigenmodes on plasma rotation has been observed, which has been explained through a redistribution of the fast ions and subsequent modification to the neutral beam torque profile. An effective momentum source has been identified by varying the input torque from neutral beam injection at fixed β_N, until the plasma rotation across the entire profile is essentially zero. This torque profile is largest near the edge, but is still non-negligible in the core, qualitatively consistent with models for a so-called 'residual stress'. Perturbative studies of the rotation using combinations of co- and counter-neutral beams have uncovered the existence of a momentum pinch in DIII-D H-mode plasmas, which is quantitatively similar to theoretical predictions resulting from consideration of low-k turbulence.

PACS numbers: 52.25.Fi, 52.55.Fa

(Some figures in this article are in colour only in the electronic version)

1. Introduction

Rotation has been shown to play a beneficial role in the confinement and stability of fusion plasmas (see, for example, [1, 2]). Since, the performance of future burning plasma devices including ITER will depend on the attained rotation profile, obtaining a predictive understanding of rotation, and ultimately exploiting such knowledge to generate an optimal rotation profile will result in a significant payoff for fusion. In effect, the goal of understanding rotation can be simplified by investigating three separate but related themes, namely that of the sources and sinks of angular momentum, plus the underlying momentum transport. Of these topics, the study of momentum transport has generally been the main focus; even still, the transport of angular momentum remains less well understood than either heat or particles.

Historically, a strong link has been observed between the thermal and momentum diffusivities [3, 4], which is expected in the presence of ion-temperature-gradient-driven turbulence [5]. However, it has also been observed that momentum transport cannot be adequately described by a purely diffusive process (e.g. [6]). In addition, theoretical treatments of momentum transport show that such 'off-diagonal' contributions to the momentum flux can manifest themselves not only as pinch-like terms [7, 8], but also act similar to a source via 'residual-stress' terms [9].

The residual stress may offer an explanation to the generation mechanism of the widely observed 'intrinsic rotation' [10–12].

Necessarily, the experimental determination of momentum transport coefficients is largely predicated on the fact that one has accurate knowledge of the sources and sinks, which is not always the case. Although neutral beam injection is the primary source of angular momentum on present-day devices, a comprehensive validation of the injected torque profile has not really be undertaken (although some aspects, such as the 'prompt' torque associated with the shift of the fast ion orbits, appear consistent with expectations [13].) The subject of momentum sinks is perhaps even less well documented, although recently, the role of non-axisymmetric magnetic fields on plasma rotation has received significant interest. Quantitative agreement [14] has been reported between experimental observations of rotation braking following application of non-resonant fields, and theory based on neoclassical flow damping [15]. The related effect of toroidal field ripple on plasma rotation has also been investigated recently [16, 17], illustrating that the entire rotation profile can be significantly modified in the presence of non-axisymmetric magnetic fields.

A coordinated effort has been undertaken on DIII-D to develop the physics basis for understanding rotation through detailed studies of the key components that determine the rotation profile. The effect of non-axisymmetric fields on plasma rotation will be discussed in section 2. Data showing the possibility of the neutral beam torque profile being modified in the presence of magnetohydrodynamic (MHD) will be shown in section 3. In section 4, evidence for an anomalous source will be presented in the context of intrinsic rotation generation. Observations of an inward pinch of momentum on DIII-D are described in section 5, and finally, in section 6 we attempt to integrate these individual physics aspects together to model the rotation profile evolution.

2. The effect of non-axisymmetric magnetic fields on plasma rotation

An often overlooked aspect of determining the rotation profile is that related to mechanisms leading to damping of angular momentum. Non-axisymmetric magnetic fields are practically unavoidable, and in some instances may be deliberately applied to the plasma for other beneficial purposes (e.g. resonant magnetic perturbations for edge-localized mode (ELM) suppression [18]). Since such fields are known to affect plasma rotation, quantitatively understanding how they do so is of considerable importance. Generally, non-axisymmetric magnetic fields (both resonant and non-resonant) are thought of as drag terms in the balance of angular momentum. In the case of resonant magnetic fields (RMFs), an electromagnetic braking torque is exerted on the plasma that can ultimately lead to a rapid collapse of the rotation once a threshold field is reached [19–21]. The torque applied by non-resonant magnetic fields (NRMFs) is predicted theoretically to take the form [15, 22]

$$\eta_{\mathrm{NRMF}} \sim -\delta B^2 \mu_{\mathrm{it}} (V_\phi - V_\phi^0), \qquad (1)$$

where δB is the NRMF, μ_{it} is an effective ion viscous damping frequency (which depends on collisionality and thereby density

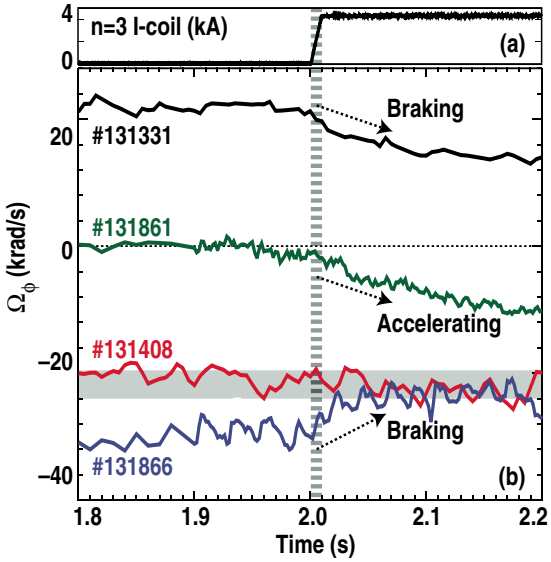

Figure 1. (*a*) Waveform of applied $n = 3$ NRMF perturbation and (*b*) time history of toroidal velocity at $\rho \sim 0.8$ for a sequence of discharges where the torque was scanned at constant β_{N}. The offset rotation is indicated by the grey band.

n_{e} and temperature T_{i}, as well as ω_{E}, the toroidal rotation driven by the radial electric field) and V_ϕ is the toroidal velocity. Here, the so-called neoclassical 'offset' velocity is given by $V_\phi^0 = (k/Z_{\mathrm{i}} e B_\theta)(\mathrm{d}T_{\mathrm{i}}/\mathrm{d}r)$, where Z_{i} is the ion charge state, B_θ is the poloidal magnetic field and k is a coefficient, also dependent on collisionality. The offset rotation is thus of the same order as the ion diamagnetic speed, and pointed in the direction counter to the plasma current, I_{p}. In specific collisionality limits, equation (1) can be written as [23]

$$\eta_{\mathrm{NRMF}} \sim -\delta B^2 n_{\mathrm{e}}^{\alpha_n} T_{\mathrm{i}}^{\alpha_T} \omega_{\mathrm{E}}^{\alpha_\omega} (V_\phi - V_\phi^0), \qquad (2)$$

where α_n, α_T and α_ω are exponents that depend on the collisionality regime limit.

Although the NRMF torque usually acts to reduce the rotation in typical experiments with large toroidal velocities resulting from uni-directional neutral beam injection, it is nonetheless the case that NRMF can actually result in a spin-up of the plasma for low toroidal velocity when $|V_\phi| < |V_\phi^0|$. Recent investigations of the effect of NRMF on toroidal rotation at DIII-D have confirmed the existence of the offset rotation [24]. NRMF are produced on DIII-D using a set of 12 coils placed around the machine in two rows of 6 (above and below the midplane), which are referred to as the I-coils.

In figure 1, NRMF are shown not only to slow the plasma rotation, but also to accelerate the plasma, depending on the initial rotation. For large initial rotation in either the co- or counter-I_{p} directions, the application of the NRMF at $t = 2.0$ s results in a braking of the plasma. However, for cases where the initial rotation is relatively low ($<50\,\mathrm{km\,s^{-1}}$), the plasma is actually observed to spin up. In all cases, the rotation tends towards the offset rotation, which for these plasmas is inferred to be approximately $50\,\mathrm{km\,s^{-1}}$ or about 1% of the local Alfvén frequency. This data set was obtained from a sequence of H-mode plasma discharges with $\beta_{\mathrm{N}} \sim 1.9$ and line average density $\bar{n}_{\mathrm{e}} \sim 4.1 \times 10^{19}\,\mathrm{m^{-3}}$. The input neutral beam torque

was varied from approximately −5.1 to 3.6 N m (negative values referring to counter-I_p), resulting in a thorough scan of the initial velocity profile. For example, at $\rho \sim 0.8$, where ρ is the normalized square root of toroidal flux, the velocity is varied from −70 to 55 km s^{-1}. In these experiments, the I-coils were configured to produce $n = 3$ NRMF, with the upper and lower coils generally connected 180° out of phase ('odd' parity), although even parity connections have also been investigated. Error correction of $n = 1$ fields is achieved using the external 'C-coils'.

Previously, plasma acceleration has been achieved using rapidly rotating resonant fields [25]. In the present experiments, by exploiting the offset rotation, it is not necessary to rotate the non-axisymmetric fields to achieve a spin-up in the rotation. In that sense, the NRMF torque can still be considered a drag, provided one appreciates that the drag is towards a finite-rotation condition. The local torque density has been computed as the time derivative of the angular momentum density $\mathrm{d}l/\mathrm{d}t$, which exhibits the offset linear relationship as expected from theory [23, 26]. In the cases where the initial plasma rotation is small, the acceleration of the plasma by the applied $n = 3$ NRMF results in an improvement in the global energy confinement. For the discharge in figure 1 starting at near zero rotation (#131861), β_N increases from approximately 1.6 before the NRMF, to 1.75 about 200 ms later, and the H-factor, H_{89}, also increases approximately 10% during this time. The rotation is found to increase significantly at all radii. The increase in rotation results in a slight increase in the $E \times B$ shearing frequency, and TGLF [27] modelling also indicates a reduction in the growth rate for ion temperature gradient modes. The increase in the shearing rate coupled with the reduction in the growth rate provides a qualitative explanation for the confinement improvement. Note that although the rotation measurement is based on the carbon impurity in the plasma, estimates of the main ion (deuterium) rotation, using NCLASS [28], show the same basic behaviour.

An immediate consequence of the existence of the offset rotation is that if the plasma is initially rotating at the offset rotation, then the application of NRMF will result in no additional torque being applied and no change in the plasma rotation. This is close to the situation in discharge #131408 in figure 1, which shows no discernible change in the rotation following the application of the NRMF at 2000 ms. Indeed, this is true across the plasma radius, and so we may approximate the offset rotation as the actual initial rotation of this discharge. This rotation, normalized by $(1/Z_i e B_\theta)(\mathrm{d}T_i/\mathrm{d}r)$, gives an experimental estimate of the radial profile of the leading coefficient k of the offset rotation, as presented in [24]. The experimentally deduced offset rotation lies between the two theoretically predicted values corresponding to the high collisionality limit (the so-called $1/\nu$-regime), with the ordering $\omega_E < \nu_i/\epsilon < \omega_{ti}\sqrt{\epsilon}$ and the ν-regime, where $\omega_E > \nu_i/\epsilon$. Nonetheless, the experimental data suggest that the connection between these two limits is highly non-linear, as indicated by the variation in k with $(\nu_i/\epsilon)/\omega_E$ in figure 3 of [24], and a continuous interpolation formula applicable for all regimes is needed for a more quantitative comparison. The existence of the offset rotation and the fact that the application of NRMF can lead to a spin up may have some important consequences, especially pertaining to the use of RMF for ELM suppression. In particular, there has been concern for ITER, where the coils proposed to produce the RMF have significant non-resonant components. Calculations have been performed of the NRMF braking associated with these components, which estimate that the torques may exceed that from the neutral beams [29]. Such estimates are particularly worrisome because of the increased likelihood of wall locking as the rotation is slowed. As a result, much effort has been focused on trying to minimize the non-resonant component of the applied field. To date, these calculations have not considered the role of the offset rotation, and its potential positive effect on plasma rotation and confinement. In light of this, one can also entertain an alternative possibility, whereby one maximizes the non-resonant components to force the plasma towards the offset rotation.

To further test our understanding of the torque generated by NRMFs, we have modelled the rotation profile evolution in the presence of a preprogrammed magnetic field perturbation. We use TRANSP [30] to follow angular momentum balance, given approximately as

$$mnR\frac{\partial V_\phi}{\partial t} = \Sigma\eta + \nabla\cdot\Gamma_\phi, \tag{3}$$

where m is the ion mass, $\Sigma\eta$ is the sum of all external torque sources, including the NRMF torque as well as the neutral beam driven torque, and the momentum flux $\Gamma_\phi = mnR\chi_\phi^{\mathrm{eff}}\partial V_\phi/\partial r$ is characterized by an effective momentum diffusivity χ_ϕ^{eff}. The torque profile deposited by the neutral beams is calculated using the NUBEAM [31, 32] package within TRANSP, which simulates and tracks a large number of Monte Carlo beam ions as they collisionally slow down in the background plasma. For the transport term, we compute χ_ϕ^{eff} immediately before the I-coil pulse and again at the completion of the application of the NRMF. We then construct a linear variation of the effective momentum diffusivity between these time points to allow for slow time scale change in the plasma transport.

For these studies, we have input the NRMF torque profile as determined from the initial $\mathrm{d}l/\mathrm{d}t$ measurement, and scaled it in time following equation (2) with $\delta B^2 \propto \delta I^2$ corresponding to the I-coil current waveform and the exponents α_n, α_T and α_ω determined from a database analysis of a set of discharges including the effect of the plasma response [33], yielding $\eta_{\mathrm{NRMF}} \sim -\delta I^2 n_e^{3.6} T_i^{2.6} \omega_E^{-0.6}(V_\phi - V_\phi^0)$. The measured $\mathrm{d}l/\mathrm{d}t$ is more uncertain inside of $\rho < 0.4$, where there is core MHD that can affect the interpretation, and so instead we extrapolate the NRMF torque profile to 0 at $\rho = 0$ from the value at $\rho = 0.4$. In addition, we account for the variation in the torque as the rotation varies due to the change in proximity to the offset rotation, which is constructed using the experimentally derived k profile. The various experimental profiles and time histories are plotted in figure 2, as well as the resulting computed NRMF torque.

The result of this analysis is shown in figure 3, which compares the measured rotation evolution across the plasma to the modelled quantity. The modelled rotation including the experimentally estimated evolution of the NRMF torque profile adequately reproduces the measured data. This is indicative that, at least in this collisionality regime, our empirical

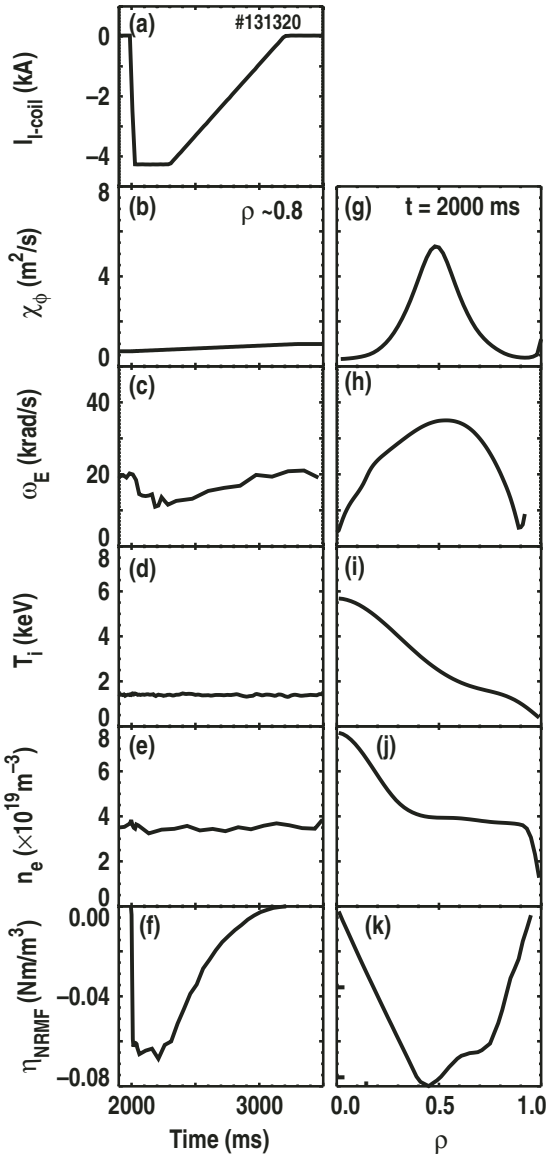

Figure 2. (*a*) Time trace of I-coil current producing $n = 3$ NRMF field, Time traces at $\rho \sim 0.8$ for (*b*) χ_ϕ, (*c*) ω_E, (*d*) T_i, (*e*) n_e and η_{NRMF} input for modelling of the rotation evolution in the presence of NRMF. (*g*)–(*k*) Corresponding profiles at $t = 2000$ ms.

information of the NRMF torque is a good representation of the actual torque generated by the NRMF. In this analysis, the role of the intrinsic analysis is ignored; however, it is not expected to play a major role in this relatively high NB torque input case. We will return to this issue in section 6.

3. Modifications to the neutral beam torque in the presence of MHD

Neutral beams are the primary source of angular momentum to DIII-D and other large fusion plasmas. Although classical transport of fast ions is included in calculations of the neutral beam driven torque in codes such as NUBEAM, MHD modes are capable of enhancing this transport, including fishbones [34], neoclassical tearing modes [35–37] and Alfvén eigenmodes (AEs) [38, 39]. In this section, we will focus on

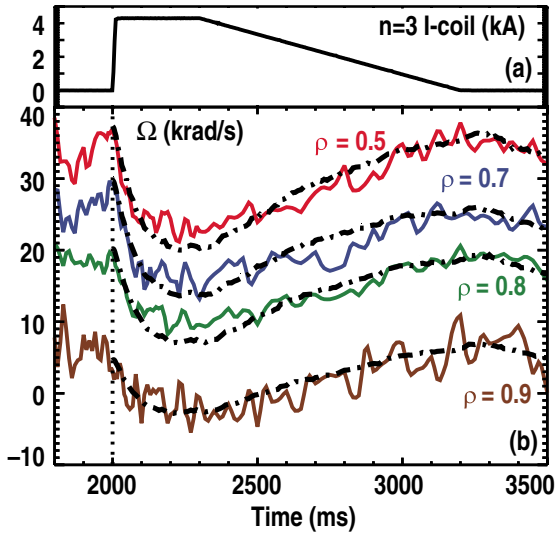

Figure 3. (*a*) I-coil current and (*b*) toroidal rotation evolution: measured (——), modelled (— · —).

the last of these, which are often observed on DIII-D and are especially pronounced at low I_p and under reverse magnetic shear conditions. These modes lead to non-classical fast ion transport, which has been shown to result in a flattening of the fast ion pressure profile. This enhanced transport of the fast ions from the hot centre is often evident even in global quantities such as the neutron production rate or stored energy. Clearly then, the presence of such modes and their associated anomalous fast ion transport may significantly alter the torque delivered by the neutral beams, making the computation of the torque profile questionable.

Experiments on DIII-D have used electron cyclotron heating (ECH) as a tool to control the level of reverse shear Alfvén eigenmode (RSAE) activity [40]. The ECH deposition radius was scanned on a shot-to-shot basis, from near the axis, to $\rho \sim 0.4$. The outer locations of this scan correspond to approximately q_{min}, the location of the minimum of the safety factor q. The total ECH power as well as the neutral beam injection was held constant across the shots. When the ECH is deposited near q_{min}, the strong RSAEs observed in these plasmas are largely suppressed, as indicated by windowed cross-power spectra between a vertical and radial CO_2 interferometer channel (e.g. figure 2 from [40]). In figure 4(*a*), the central toroidal rotation as a function of time is plotted for two discharges at low current during the I_p ramp phase; one with strong RSAE activity, the other with the RSAEs suppressed. In addition, both discharges have significant toroidicity-induced Alfvén eigenmode (TAE) activity, but to a first approximation this activity is unchanged for the two cases. In the case with reduced RSAE activity, the rotation is almost a factor of two higher. We find that the angular momentum density profile is more peaked when the RSAEs are suppressed, yet interestingly, the total integrated angular momentum in the plasma for the two cases is relatively unchanged (figure 4(*b*)).

The change in rotation can be attributed to two distinct physics mechanisms. The first, and the usual consideration, is that the underlying momentum transport is different between the two discharges. Such changes can result from even subtle

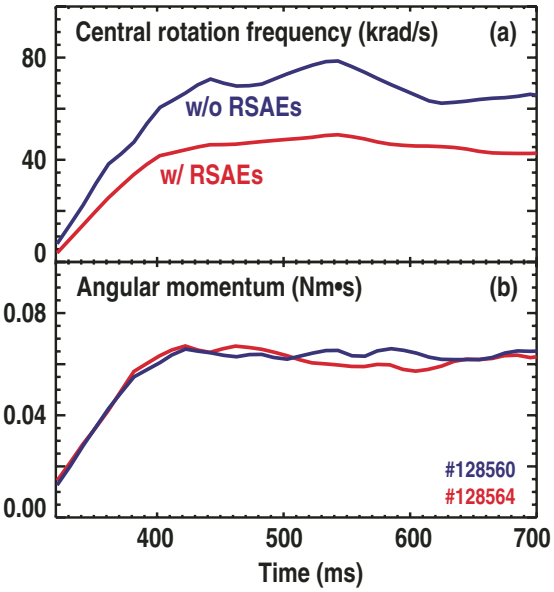

Figure 4. (*a*) Central rotation frequency and (*b*) angular momentum content of comparison discharges with and without RSAEs.

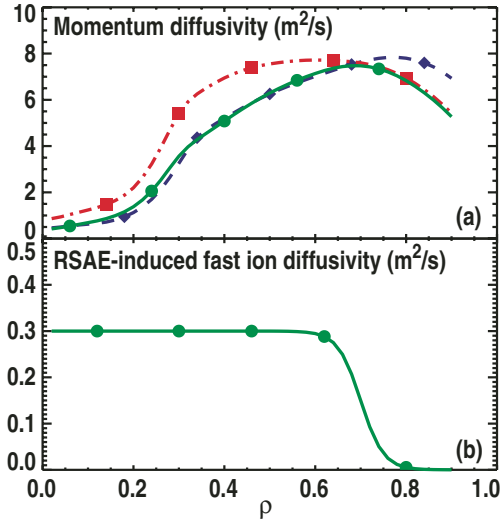

Figure 5. (*a*) Radial profiles at $t = 600$ ms of the computed momentum diffusivity for comparison discharges with (— · —) and without (- - - -) RSAEs. (*b*) Assuming an anomalous fast ion diffusivity resulting from enhanced RSAE-induced fast ion transport, the underlying momentum diffusivity in the core for the discharge with RSAEs is recovered (——).

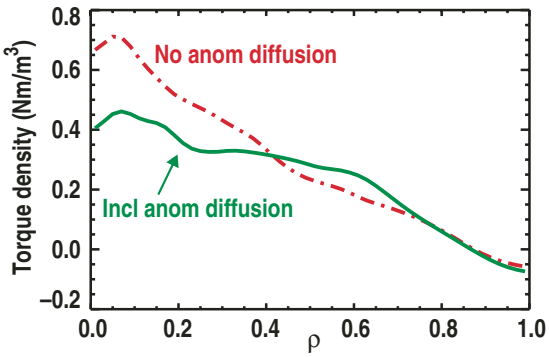

Figure 6. Calculated torque profile from TRANSP assuming classical fast ion diffusion (— · —) and using RSAE-enhanced fast ion diffusion inferred from momentum transport considerations (——).

changes to the profiles. For these two discharges, most profiles are actually relatively similar, including the q-profile; however, due to the different ECH deposition, the T_e profile is notably different. Hence, changes in transport may well be responsible for the observed changes in the rotation, although it would be somewhat unusual for these local transport changes to manifest themselves in such a way that the total angular momentum remained the same. An alternative possibility is that the underlying momentum source has been modified due to the RSAE activity. The fact that the total angular momentum is approximately the same suggests that any such source modification would appear as a redistribution of the fast ion profile, rather than a complete loss of fast ions per se, which is qualitatively consistent with the behaviour expected from the relatively localized RSAEs. Of course, some combination of both effects may be present. For now, we will consider that the second effect is dominant, and investigate whether such changes are consistent with other observations.

The momentum diffusivity profile is deduced using TRANSP, from the rotation profile evolution and calculated torque profiles, assuming classical fast ion transport. The result is shown in figure 5(*a*). The effective momentum diffusivity $\chi_\phi^{\rm eff}$ in the core, $\rho < 0.7$, is considerably larger for the discharge with RSAE activity. If we believe that the source profile being calculated in TRANSP is incorrect due to the enhanced fast ion transport associated with the RSAEs, then this change in the momentum diffusivity is merely an artefact of having the wrong source profile. TRANSP includes the option for ad hoc anomalous fast ion transport, which was used to deduce the enhancement of fast ion transport due to the RSAEs, by better matching the $\chi_\phi^{\rm eff}$ profiles for the two shots. We find that the anomalous fast ion diffusion as shown in figure 5(*b*), with a value of $\chi_{\rm FI} \sim 0.3\,{\rm m}^2\,{\rm s}^{-1}$ in the core, and falling to zero at the edge, best modifies the inferred $\chi_\phi^{\rm eff}$ profile for the RSAE discharge to match the shot without RSAEs.

If such enhanced fast ion transport is actually present as suggested by angular momentum considerations, then the torque delivered by the neutral beams is substantially altered. In particular, there is a reduction in the on-axis torque by approximately 40%, as shown in figure 6. Enhanced fast ion diffusion can modify the torque profile in two distinct ways. When the fast ions are transported, the location where they collisionally slow down on the thermals and deliver torque is obviously changed. However, a more subtle effect is realized in the bookkeeping of charge neutrality within TRANSP, where the outward transport of the fast ions is balanced by an inward return current of thermal ions. These inward moving thermal ions experience a $j \times B$ torque in the counter-I_p direction. It is through this same basic principle that the angular momentum delivered to the plasma by a counter neutral beam can significantly exceed the angular momentum of the beam [41]. However, for the RSAE-enhanced fast ion diffusion, the existence of this secondary $j \times B$ torque is model dependent. If charge neutrality is instead maintained through increased electron transport, then this extra counter-torque will not be realized. At present, it is not clear which of the two

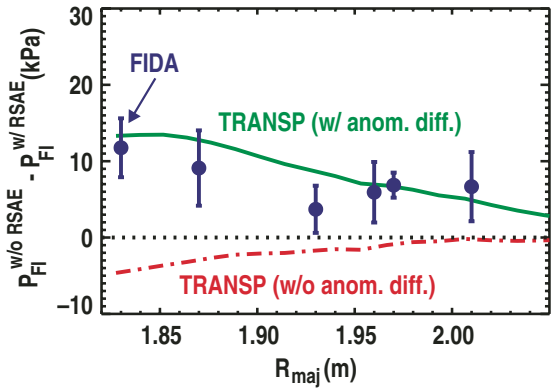

Figure 7. Difference in fast ion pressure between discharges without RSAEs versus with RSAEs, calculated classically (— · —) and including the deduced RSAE-induced fast ion transport (——). Comparison with FIDA measurements is also shown.

cases related to the $j \times B$ torque is the reality (or indeed, whether perhaps it is somewhere in between these extremes). Nonetheless, the torque modification presented in figure 6 results almost entirely from changes to the collisional torque, and the model-dependent $j \times B$ torque change is relatively insignificant. However, in analysis presented in later sections, this distinction will be more important.

The deduced RSAE enhancement of the fast ion transport is supported by other measurements. The AE activity present in both discharges results in the measured neutron rates being well below the TRANSP calculation based on classical fast ion transport, but the shot with RSAEs is notably worse (a further 25% reduction). This additional deficit can be adequately explained in TRANSP calculations using the above mentioned anomalous fast ion transport. The fast ion pressure is also significantly reduced by the deduced anomalous fast ion transport. Classically, the two discharges are expected to have similar fast ion pressures on axis (to within about 10%). The fast ion profiles from the fast ion D_α (FIDA) diagnostic [42] were measured for these two discharges and the difference between them is shown in figure 7. The FIDA signal is a result of a convolution of a 'weight function' with the fast ion distribution function [43]. For the range of wavelengths considered in the FIDA analysis (corresponding to energies from about 30 to 60 keV), the weight function favours densities in the high energy region of the distribution function, and due to the near constant effective temperature of the fast ions, the FIDA signal can be considered a proxy for the fast ion pressure. In this particular analysis, the relatively calibrated FIDA signals are scaled by a single constant such that the central FIDA 'pressure' matches that from the discharge with no RSAEs. The FIDA measurements indicate that the shot with RSAEs has lower fast ion pressure, and the measured difference in pressure between the two discharges is in reasonable agreement with the calculated difference when the inferred anomalous fast ion transport from figure 5(*b*) is included. In light of the impact of non-classical fast ion transport on the deposited torque profile, it is clear that more careful validation of the computed neutral beam torque profiles from codes like TRANSP is required as part of the effort to gain predictive knowledge of plasma rotation in future devices.

4. Generation of intrinsic rotation

The physics pertaining to the generation of the so-called 'intrinsic' rotation [10–12], which refers to plasma rotation in the absence of any auxiliary torque input, is currently not well understood. Therefore, in addition to readily identifiable sources of angular momentum to the plasma such as neutral beams, rotation studies have more recently had to confront the existence of additional effective source(s) of rotation. While the existence of intrinsic rotation has been demonstrated in several tokamaks, the role of intrinsic rotation in the presence of strong neutral beam injection has not been investigated as thoroughly.

Torque scans at constant β_N have been conducted in ELMing H-mode with $\beta_N \sim 1.7 \pm 10\%$ and elevated q_{min} to investigate intrinsic rotation and momentum transport [44]. Across the entire profile, we find a residual co-rotation in the plasma, even when the neutral beams are nominally balanced. This rotation at zero net torque is related to the intrinsic rotation, although it is somewhat more complicated to interpret due to the details of the individual neutral beam torque profiles (specifically, due to the different deposition profiles for co- and counter-beams, net 'balanced' torque invariably implies regions of both co- and counter-torque densities across the plasma radius). Perhaps more definitive evidence of the intrinsic rotation comes then from the fact that the rotation profile remains peaked and in the co-I_p direction even when the total torque is negative (meaning in the counter I_p direction), and the torque deposition profile is essentially zero from $0 < \rho < 0.7$ and negative beyond that. Although the rotation data come from impurity carbon measurements, the neoclassical corrections for the main ion deuterium tend to further increase the amount of co-rotation.

Evidence of the role of intrinsic rotation in the presence of neutral beam input is clearly indicated in figure 8(*a*), showing the toroidal rotation frequency profile at two times during a discharge in which the beam balance went from 3 co-neutral beams to 1 net counter beam (produced from 2 counter + 1 co-beam). In the later time, the rotation profile is effectively zero everywhere and steady for several hundred milliseconds, despite the fact that there is one net counter source. The momentum flux can be written more completely as

$$\Gamma_\phi = -mnR\left(\chi_\phi \frac{\partial V_\phi}{\partial r} - V_{\text{pinch}} V_\phi\right) + \Gamma_{\text{RS}}, \qquad (4)$$

to allow for an angular momentum pinch velocity V_{pinch} and other 'residual stress' fluxes Γ_{RS} [9], in addition to the momentum diffusivity χ_ϕ. Following from the momentum balance equation as in equation (3), it is evident that for the case where the rotation is zero everywhere across the profile and not evolving, then the net source must be balanced by the residual stress, $\nabla \cdot \Gamma_{\text{RS}} = -\Sigma\eta$. In other words, the residual stress acts as an effective torque, $\eta_{\text{effective}}$, opposing the neutral beam torque. In this specific case, where there is one net counter neutral beam, this effective torque must integrate to approximately one co-source.

The deduced effective torque in these plasmas is shown in figure 8(*b*). The neutral beam torque profile is calculated assuming classical fast ion transport, although as highlighted in the previous section, such assumptions are likely too

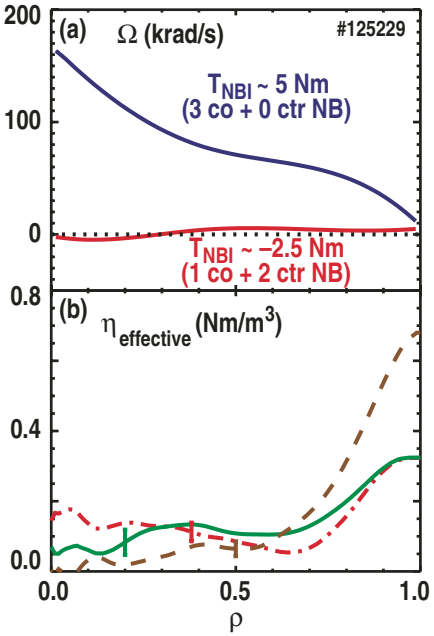

Figure 8. (*a*) Change in rotation frequency profile going from three co-sources to one co-plus two counter. (*b*) The effective torque profile associated with the intrinsic rotation is inferred differently depending on the level and nature of anomalous fast ion transport: no anomalous fast ion diffusion (— · —); flat anomalous fast ion diffusion (——); and flat diffusion including additional non-ambipolar $j \times B$ driven torque (- - - -).

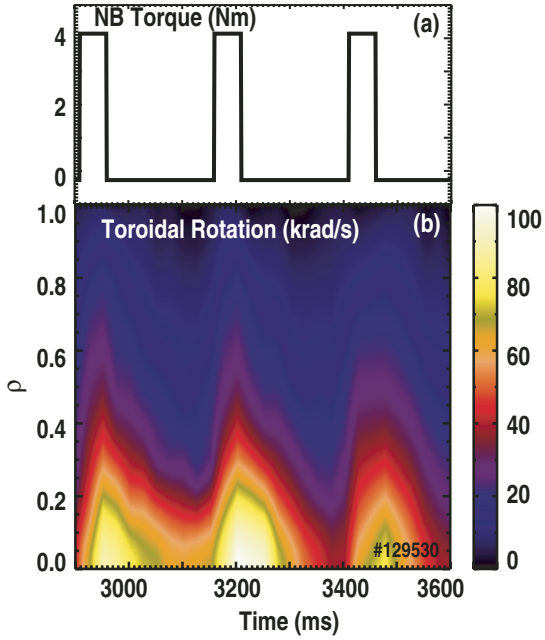

Figure 9. (*a*) Co-NBI blips applied at constant power for a duration of 50 ms, with 200 ms between blips. (*b*) Corresponding perturbation to the rotation profile.

simple. Indeed, these discharges show a variety of AEs, and the classically predicted neutron rate is 25–30% above the measured quantity. Allowing flat anomalous fast ion diffusion profiles to account for this discrepancy in the neutrons modifies the inferred effective torque profile as described in section 3. However, unlike the shot presented in that section, here there is a notable difference between whether or not one includes the additional $j \times B$ torque that is generated in the case of a radial inward return current. These two situations, which in some sense may represent two extremes in the effective torque profile, are also included in figure 8. In both cases, the torque becomes relatively more peaked at the edge, qualitatively consistent with the concept of residual stress driven by strong gradients in the $E \times B$ velocity [9] utilizing parallel wavenumber symmetry breaking [45], as well as models due to thermal ion orbit loss [46]. A hint of the existence of an effective torque has also been observed during transient analysis of rotation data on JFT-2M [6].

5. Momentum transport

Finally, we turn to the role of momentum transport in the determination of the rotation profile. Momentum transport is generally found to be largely anomalous relative to neoclassical predictions, even in cases where the ion thermal transport has been reduced to neoclassical levels due to strong $E \times B$ stabilization of long wavelength turbulence [47]. Therefore, in some ways, momentum transport remains the least well understood of all the transport channels, and the characterization of momentum transport leading to fundamental understanding of the anomalous transport mechanism is sorely needed. Non-linear gyrokinetic codes such as GYRO [48] and GTS [49] have now reached a level of completeness to properly begin to address momentum transport. In this respect, experimental observations of momentum transport are valuable in guiding theoretical and modelling studies.

Although momentum transport has commonly been characterized as a purely diffusive process, perturbative studies of the rotation using combinations of co- and counter-neutral beams have revealed the existence of a momentum pinch in DIII-D H-mode plasmas. In particular, a train of neutral beam 'blips' is fired into the plasma at constant power. Each blip is 50 ms long, which is short compared with the confinement time, but long enough to have a measurable effect on the rotation as shown in figure 9. The plasma is then given 200 ms between blips to recover. The viscous angular momentum flux is inferred from angular momentum balance (equation (3)) in TRANSP during the rotation relaxation following the NB blip perturbations. One must appreciate that the inferred flux is intimately related to accurately characterizing the sources and sinks as discussed in the previous sections, and given the relatively large unknowns in these terms, momentum transport studies can be consequently somewhat uncertain. To some extent, we alleviate these problems with perturbative studies; for example, at constant β_N we should expect that the effective torque associated with the intrinsic rotation described in section 4 is not significantly changed based on the present ideas about the scaling of intrinsic rotation. If we have residual error fields dragging on the plasma, then these too should be relatively unchanged by our perturbations, although the resultant NRMF torque may still modulate with the toroidal velocity according to equation (2). Even assuming that the intrinsic error field is as large as our applied fields in section 2, the NRMF torque modulation is still at least a factor of 4–5

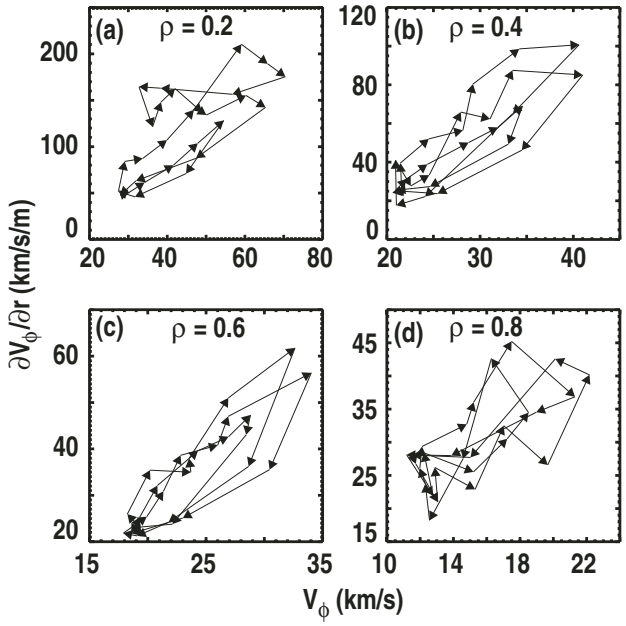

Figure 10. Elliptical trajectories of $\partial V_\phi/\partial r$ versus V_ϕ during NBI perturbations, for (*a*) $\rho = 0.2$, (*b*) $\rho = 0.4$, (*c*) $\rho = 0.6$, (*d*) $\rho = 0.8$.

smaller than that from the beams and vanishes rapidly with presumably smaller residual error fields as δB^2.

In order to successfully separate out the diffusive and pinch components to the momentum flux, the rotation perturbation must result in the velocity changing independent of its radial gradient, so that there is a decoupling of these two terms of the momentum flux in equation (4). In these experiments, plots of V_ϕ versus $\partial V_\phi/\partial r$ result in elliptical trajectories as shown in figure 10, suitable for such decomposition.

The flow of momentum (in Nm) through a given radius is given by the volume integral of the experimentally inferred momentum flux, $\int_0^\rho \nabla\cdot\Gamma_\phi \, dV$, which is shown in figure 11, for $\rho = 0.4$ values for a low rotation H-mode plasma. Using a non-linear least squares fitter, we find time-invariant profiles for χ_ϕ and $V_{\rm pinch}$, which, when used in equation (4), best reproduce the measured flow following the NB blip perturbations. The match to the data is also plotted in figure 11, considering individually a purely diffusive model (i.e. explicitly forcing $V_{\rm pinch} \equiv 0$) versus one including a momentum pinch. One can see that there is insufficient freedom in the fit of the experimental flow with only diffusion. In particular, such a model fails when the velocity gradient is zero while the flow remains finite (e.g. around $t = 3.8$ s in figure 11). Effectively, the diffusive-only flow is constrained to zero at such times, resulting in an offset to the experimental flow and a poor fit overall. The fit is notably better when finite $V_{\rm pinch}$ is allowed. Indeed, a statistically significant improvement is found at all radii, as indicated by the lowering of the reduced-χ^2 when $V_{\rm pinch}$ is included in the fit.

In these studies, we infer an inward pinch of momentum, given by the negative sign in figure 12. The pinch velocity tends to be relatively small, generally less than 10 m s^{-1} until the outer third of the plasma. Even still, including the pinch notably changes the inferred χ_ϕ profile, which can easily increase a factor of 2 or more. The change is more pronounced

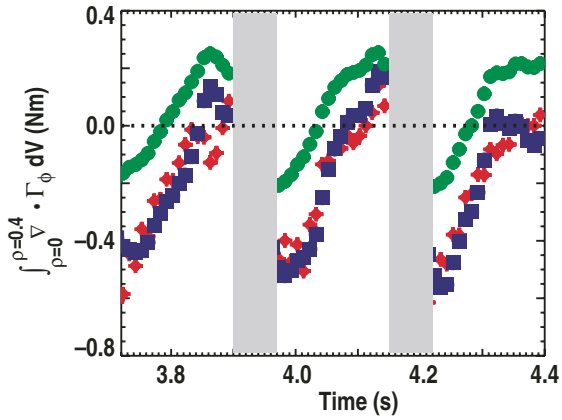

Figure 11. Experimentally inferred evolution of the momentum flow integrated to $\rho = 0.4$ (diamond). Modelled evolution, assuming $V_{\rm pinch} \equiv 0$ (circle), and allowing finite $V_{\rm pinch}$ (square).

at low rotation, where the transport is presumably relatively poor due to reduced $E \times B$ shear. It should therefore be noted that an effective χ_ϕ is unlikely to be satisfactory for prediction of the rotation profile. Such an inward pinch of momentum has also been seen on JT-60U [50], JET [51] and NSTX [52].

The inferred inward momentum pinch velocity from this analysis shows quantitative similarity to theoretical predictions resulting from consideration of low-k turbulence by Hahm *et al* [7], $V_{\rm pinch} = -(4 + R/L_n)\chi_\phi/R$ and Peeters *et al* [8] $V_{\rm pinch} = \chi_\phi/R(-4 - R/L_n)$, where L_n is the density gradient scale length. A comparison of the inferred pinch velocity with theoretical predictions is shown in figure 13 for the low rotation, low $E \times B$ shear plasma, where low-k turbulence can be expected to play a larger role. Favourable agreement is observed across much of the profile with both theories in this case, although worse agreement is generally found for higher rotation cases. The Peeters form of the pinch velocity appears to do better in the limited region $0.7 < \rho < 0.8$, where the L_n begins to make a relatively larger contribution, however, notable discrepancy outside of $\rho > 0.8$ still needs to be understood. This may be explainable by other quantities contributing to the pinch velocity as suggested by gyrokinetic simulations, or may simply be a result of imperfect stationarity of the edge intrinsic torque during the modulation. Similar results have also been obtained on NSTX [52], which has shown a more clear dependence of the pinch velocity on L_n.

6. Integrated modelling of the angular momentum profile evolution

Ultimately, the rotation profile depends on the interplay between sources, sinks and transport as dictated by angular momentum balance, equation (3). To begin to address this complicated issue, we have attempted to extend the modelling presented in section 2 to a low rotation discharge, where the effective torque associated with the intrinsic rotation as discussed in section 4 becomes a significant player. This discharge also has notable MHD activity resulting in a large discrepancy in the neutron production and equilibrium stored energy, evidence of enhanced fast ion transport that can affect the NB-driven torque profile as described in section 3. This

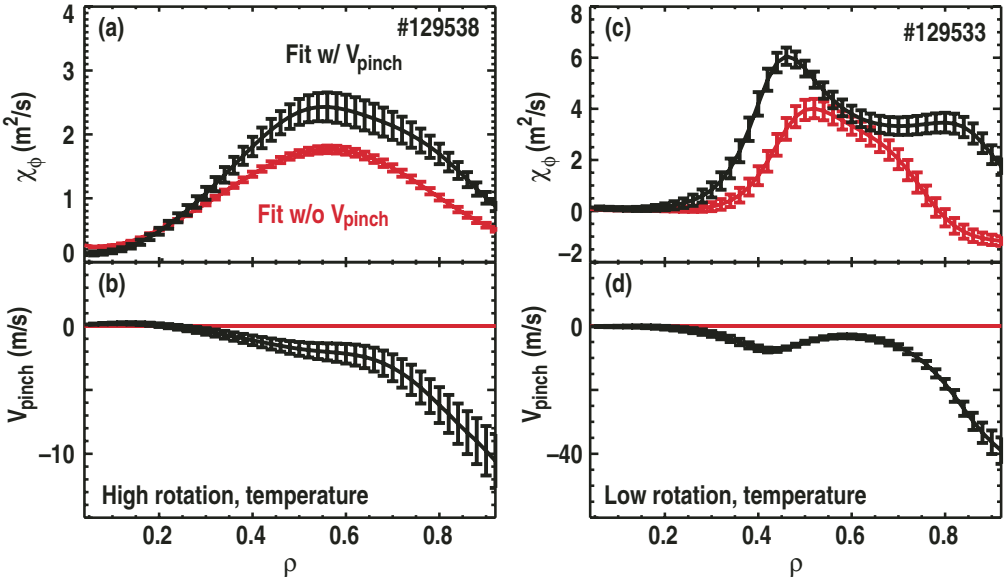

Figure 12. (*a*) Momentum diffusivity and (*b*) pinch velocity inferred from perturbation experiment for a high rotation/temperature discharge. For comparison, the effective momentum diffusivity is also shown for $V_{pinch} \equiv 0$. Corresponding (*c*) momentum diffusivity and (*d*) pinch velocity for low rotation discharge.

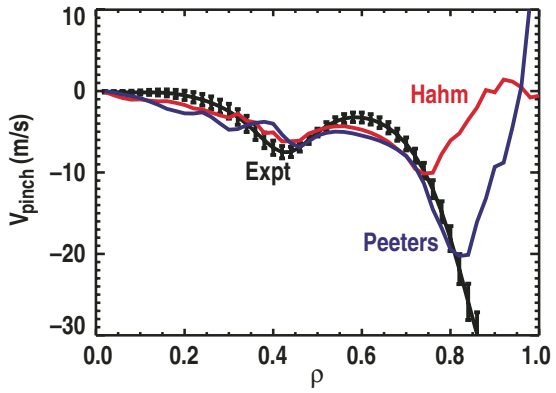

Figure 13. Experimentally determined pinch velocity from perturbation experiment compared with theory of Hahm *et al* [7] and Peeters *et al* [8].

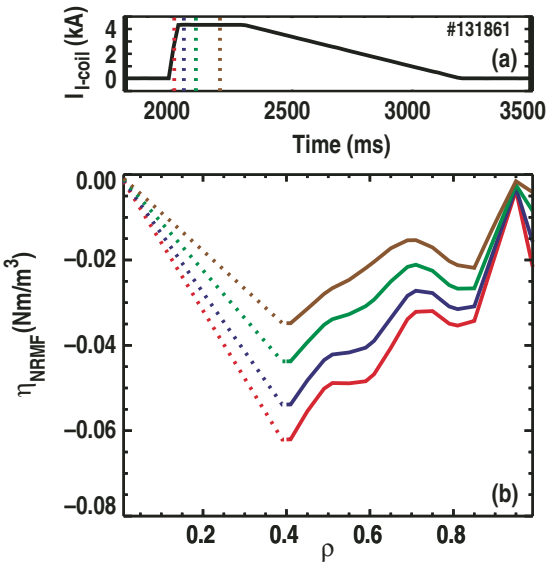

Figure 14. (*a*) Applied $n = 3$ NRMF perturbation. (*b*) Evolution of the NRMF torque profile at times indicated in (*a*), $t = 2010$, 2050, 2100 and 2200 ms. Due to the rapid change in rotation and relative proximity to the offset rotation, the torque drops rapidly, and is reduced almost a factor of 2 after ∼200 ms even though the applied field is constant.

discharge is also of particular interest, since it represents a case where NRMF is used to accelerate the plasma from essentially rest.

Similar to the modelling in section 2, the initial NRMF torque profile at $t = 2000$ ms is computed from the measured inertial response $\mathrm{d}I/\mathrm{d}t$ and evolved according to the I-coil waveform and other measured data as described by equation (2). However, unlike the case in section 2, here the rotation is much lower putting us in the $1/\nu$-regime. Unfortunately, the database studies in [33] do not extend to this collisionality regime. Nonetheless, in the $1/\nu$-regime, there is not expected to be any dependence on ω_E (i.e. $\alpha_\omega \equiv 0$), so we have omitted ω_E from this analysis. Moreover, given that both n_e and T_i are close to constant, we can neglect these dependences also. The $V_\phi - V_\phi^0$ dependence, however, is retained, and is especially important here (although there is now some uncertainty in V_ϕ^0 due to the change in collisionality). This is illustrated in figure 14, which shows the initial NRMF torque profile and subsequent time slices. Note that due to the initial rapid acceleration of the plasma towards the offset rotation, the torque is consequently strongly reduced.

As described in [44], the characterization of even the global momentum confinement time τ_ϕ at low rotation becomes extremely problematic due to the unaccounted momentum flux associated with the intrinsic rotation. For example, in steady state, $\tau_\phi = L/\Sigma T$, where L is the total angular momentum and ΣT is the sum of the applied torque. In this case, the total delivered NB torque is estimated to be -3.3 N m including estimated anomalous fast ion diffusion consistent with the neutron rate and stored energy as described

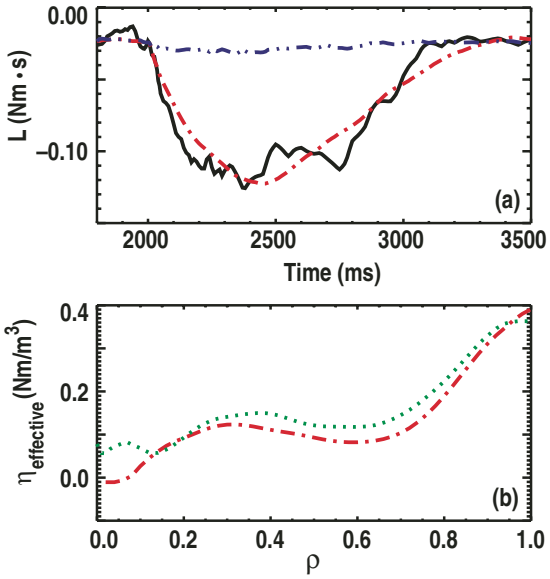

Figure 15. (*a*) Experimentally determined (——) angular momentum compared with modelled result, neglecting the effective torque associated with the intrinsic rotation (— · · —). The modelled agreement is significantly improved (— · —) when including the corresponding effective intrinsic torque in (*b*). For comparison, the effective torque profile inferred from steady state analysis in figure 8, scaled up by 10% to correct for the difference in β_N, is also shown (· · · · · ·).

in section 3, yet the total angular momentum is merely −0.02 N m s, resulting in a very short $\tau_\phi \sim 7$ ms, much shorter than the energy confinement time, $\tau_E > 50$ ms. The apparently poor momentum confinement results from the unaccounted intrinsic rotation, which effectively opposes the counter NB injection here, resulting in low rotation.

We can readily verify that there is significant intrinsic rotation and that the momentum confinement is not as poor as the above crude estimate might suggest, by investigating the time rate of change in angular momentum following the application of the NRMF. We can integrate the global angular momentum balance equation

$$\frac{dL}{dt} = \Sigma T - \frac{L}{\tau_\phi}, \tag{5}$$

to determine the angular momentum evolution, with the total torque given by the sum of the neutral beam and NRMF torques, $\Sigma T = T_{NBI} + T_{NRMF}$, neglecting the intrinsic rotation. To allow for transport changes during the acceleration, we take our inferred τ_ϕ from before the NRMF pulse at $t = t_0 = 2000$ ms and scale it with the variation in τ_E, i.e. $\tau_\phi(t) = [\tau_\phi(t_0)/\tau_E(t_0)]\tau_E(t)$. The result is shown in figure 15, comparing the modelled response assuming τ_ϕ determined neglecting the intrinsic rotation, with the actual measured angular momentum evolution. While the initial acceleration is captured over the first ∼20 ms (consistent with the dI/dt inference of the torque), the rest of the modelled time history shows little resemblance to the data. With such a short momentum confinement time, the NRMF torque has relatively little impact on the rotation, and the angular momentum remains relatively close to zero.

Hence, in order to model the rotation evolution, we must account for the intrinsic rotation. In the global angular momentum balance equation, this can be achieved most readily by including an effective source term for the intrinsic rotation, such that $\Sigma T = T_{NBI} + T_{NRMF} + T_{effective}$. The inclusion of $T_{effective}$ will alter our inference of the initial momentum confinement $\tau_\phi(t_0)$. Given that L is very small before the NRMF is applied, we may expect that $T_{effective} \approx -T_{NBI}$. In other words, our estimate of τ_ϕ and the resultant modelling of the rotation is extremely sensitive to the value chosen for $T_{effective}$. To deal with this, we reverse the problem, and instead use a non-linear least squares fitter to find the level of intrinsic torque required for the modelled angular momentum evolution to match the data, which assumes that we know how to properly compute the NRMF torque as demonstrated in section 2. We find that an effective intrinsic torque of 3.2 N m is required to match the measured angular momentum evolution, also shown in figure 15(*a*).

Following exactly the same procedure, we can 'peel' shells off the plasma, integrating the angular momentum and torque densities up to successively smaller ρ values, thereby inferring the integrated effective intrinsic torque to the same radius. From this profile, we can then back out the intrinsic torque density, the result of which is plotted in figure 15(*b*). For comparison, the intrinsic torque profile estimated in section 4 is also plotted, scaled up following the 'Rice' scaling [53] uniformly by approximately 10% to account for the slightly higher β_N. Relatively good agreement is found with the intrinsic source estimated using the steady state analysis approach in section 4 across the profile, again indicating the localization of the torque to the edge. This internal consistency for the inferred intrinsic torque can be taken as a sign of success that the individual aspects affecting rotation as outlined in sections 2 through 4 can be integrated and understood as a whole. On the other hand, one must remain mindful of the fact that most of this analysis is based on empirical experimental evidence rather than first principles theoretical and/or modelling results. Until we can make that final crucial step, we cannot truly claim to have predictive knowledge of rotation.

7. Conclusions

A considerable amount of progress required to obtain predictive knowledge of rotation has been made by investigating the individual roles of sources, sinks and transport. A theoretical prediction on the existence of an offset rotation, towards which the non-resonant fields 'drag' the plasma rotation, has been experimentally confirmed for the first time. The fact that this offset rotation is non-zero opens up the possibility of using NRMFs as a means of driving toroidal rotation in fusion plasmas. New measurements have been made to characterize the modification to neutral beam torque profiles in the presence of AE activity, and the profile of the effective torque responsible for intrinsic rotation has also been directly measured. These various components have been successfully integrated to model the rotation evolution.

Acknowledgments

This work was supported by the US Department of Energy under DE-AC02-76CH03073, DE-FC02-04ER54698, DE-FG02-89ER53296, SC-G903402, DE-FG02-89ER53297 and DE-FG02-92ER54139. The authors would like to thank P.H. Diamond, T.S. Hahm and R.E. Waltz for useful discussions.

References

[1] Burrell K.H. 1997 *Phys. Plasmas* **4** 1499
[2] Strait E.J. *et al* 1995 *Phys. Rev. Lett.* **74** 2483
[3] Scott S.D. *et al* 1990 *Phys. Rev. Lett.* **64** 531
[4] DeGrassie J.S. *et al* 2003 *Nucl. Fusion* **43** 142
[5] Mattor N. and Diamond P.H. *Phys. Fluids* **31** 1180
[6] Ida K. *et al* 1995 *Phys. Rev. Lett.* **74** 1990
[7] Hahm T.S. *et al* 2007 *Phys. Plasmas* **14** 072302
[8] Peeters A.G. *et al* 2007 *Phys. Rev. Lett.* **98** 265003
[9] Gürcan Ö.D. *et al* 2007 *Phys. Plasmas* **14** 042306
[10] Eriksson L.G. *et al* 1997 *Plasma Phys. Control. Fusion* **39** 27
[11] Rice J.E. *et al* 1998 *Nucl. Fusion* **38** 75
[12] DeGrassie J.S. *et al* 2004 *Phys. Plasmas* **11** 4323
[13] DeGrassie J.S. *et al* 2006 *Phys. Plasmas* **13** 112507
[14] Zhu W. *et al* 2006 *Phys. Rev. Lett.* **96** 225002
[15] Shaing K.C. 2003 *Phys. Plasmas* **10** 1443
[16] Yoshida M. *et al* 2006 *Plasma Phys. Control. Fusion* **48** 1673
[17] de Vries P.C. *et al* 2008 *Nucl. Fusion* **48** 035007
[18] Evans T.E. *et al* 2004 *Phys. Rev. Lett.* **92** 235003
[19] Jensen T.H. 1993 *Phys. Fluids* B **5** 1239
[20] Fitzpatrick R. 1998 *Phys. Plasmas* **5** 3325
[21] Garofalo A.M. *et al* 2007 *Nucl. Fusion* **47** 1121
[22] Callen J.D. *et al* 2008 *Proc. 22nd Int. Conf. on Fusion Energy 2008 (Geneva, Switzerland, 2008)* (Vienna: IAEA) CD-ROM file th_p8-36.pdf and http://www-naweb.iaea.org/napc/physics/FEC/FEC2008/html/index.htm 2009 *Nucl. Fusion* submitted
[23] Cole A.J. *et al* 2008 *Phys. Plasmas* **15** 056102
[24] Garofalo A.M. *et al* 2008 *Phys. Rev. Lett.* **101** 195005
[25] Finken K.H. *et al* 2005 *Phys. Rev. Lett.* **94** 015003
[26] Cole A.J. *et al* 2007 *Phys. Rev. Lett.* **99** 065001
[27] Staebler G.M. *et al* 2005 *Phys. Plasmas* **12** 102508
[28] Houlberg W.A. *et al* 1997 *Phys. Plasmas* **4** 3230
[29] Becoulet M. *et al* 2008 *Proc. 22nd Int. Conf. on Fusion Energy 2008 (Geneva, Switzerland, 2008)* (Vienna: IAEA) CD-ROM file th_2-1ra.pdf and http://www-naweb.iaea.org/napc/physics/FEC/FEC2008/html/index.htm 2009 *Nucl. Fusion* submitted
[30] Hawryluk R. 1980 *Physics Plasmas Close to Thermonuclear Conditions* vol 1 ed B. Coppi *et al* (Brussels: CEC) pp 19–46
[31] Goldston R.J. *et al* 1981 *Comput. Phys. Commun.* **43** 61
[32] Pankin A. *et al* 2004 *Comput. Phys. Commun.* **159** 157
[33] Garofalo A.M. *et al* 2009 *Phys. Plasmas* **16** 056119
[34] White R.B. *et al* 1983 *Phys. Fluids* **26** 2958
[35] Zweben S.J. *et al* 1999 *Nucl. Fusion* **39** 1097
[36] Carolipio E.M. *et al* 2002 *Nucl. Fusion* **42** 853
[37] Garcia-Muñoz M. *et al* 2007 *Nucl. Fusion* **47** L10
[38] Heidbrink W.W. *et al.* 2007 *Phys. Rev. Lett.* **99** 245002
[39] Heidbrink W.W. *et al* 2008 *Nucl. Fusion* **48** 084001
[40] Van Zeeland M.A. *et al* 2008 *Plasma Phys. Control. Fusion* **50** 035009
[41] Helander P. *et al* 2005 *Phys. Plasmas* **12** 112503
[42] Luo Y. *et al* 2007 *Rev. Sci. Instrum.* **78** 033505
[43] Heidbrink W.W. *et al* 2007 *Plasma Phys. Control. Fusion* **49** 1457
[44] Solomon W.M. *et al* 2007 *Plasma Phys. Control. Fusion* **49** B313
[45] Dominguez R.R. and Staebler G.M. 1993 *Phys. Fluids* B **5** 3876
[46] DeGrassie J.S. *et al* 2008 *Proc. 22nd Int. Conf. on Fusion Energy 2008 (Geneva, Switzerland, 2008)* (Vienna: IAEA) CD-ROM file ex_p5-2.pdf and http://www-naweb.iaea.org/napc/physics/FEC/FEC2008/html/index.htm 2009 *Nucl. Fusion* submitted
[47] Kinsey J.E. *et al* 2002 *Phys. Plasmas* **9** 1676
[48] Candy J. *et al* 2003 *J. Comput. Phys.* **186** 545
[49] Wang W.X. *et al* 2006 *Phys. Plasmas* **13** 092505
[50] Yoshida M. *et al* 2007 *Nucl. Fusion* **47** 856
[51] Tala T. *et al.* 2007 *Plasma Phys. Control. Fusion* **49** B291
[52] Solomon W.M. *et al* 2008 *Phys. Rev. Lett.* **101** 065004
[53] Rice J.E. *et al* 2001 *Nucl. Fusion* **41** 277